Proc. Natl. Acad. Sci. USA
Vol. 93, pp. 6425–6430, June 1996
Medical Sciences

Whole body positron emission tomography imaging of simian immunodeficiency virus-infected rhesus macaques

(AIDS/pathogenesis/reticuloendothelial system/immunopathology/animal model)

ALEXANDER M. SCHARKO*, SCOTT B. PERLMAN†, PAUL W. HINDS II‡, JOAN M. HANSON†, HIDEO UNO‡, AND C. DAVID PAUZA*‡§

*Department of Pathology and Laboratory Medicine, ‡Wisconsin Regional Primate Research Center, and †Department of Nuclear Medicine and PET Imaging Center, University of Wisconsin, Madison, WI 53706

Communicated by Henry Lardy, University of Wisconsin, Madison, WI, March 19, 1996

ABSTRACT **Pathogenesis of simian immunodeficiency virus (SIV) infection in rhesus macaques begins with acute viremia and then progresses to a distributed infection in the solid lymphoid tissues, which is followed by a process of cellular destruction leading to terminal disease and death. Blood and tissue specimens show the progress of infection at the cellular level but do not reveal the pattern of infection and host responses occurring throughout the body. The purpose of this investigation was to determine whether positron emission tomography (PET) imaging with intravenous 2-^{18}F-2-deoxyglucose (FDG) could identify activated lymphoid tissues in a living animal and whether this pattern would reflect the extent of SIV infection. PET images from SIV-infected animals were distinguishable from uninfected controls and revealed a pattern consistent with widespread lymphoid tissue activation. Significant FDG accumulation in colon along with mesenteric and ileocaecal lymph nodes was found in SIV infection, especially during terminal disease stages. Areas of elevated FDG uptake in the PET images were correlated with productive SIV infection using *in situ* hybridization as a test for virus replication. PET-FDG images of SIV-infected animals correlated sites of virus replication with high FDG accumulation. These data show that the method can be used to evaluate the distribution and activity of infected tissues in a living animal without biopsy. Fewer tissues had high FDG uptake in terminal animals than midstage animals, and both were clearly distinguishable from uninfected animal scans.**

Microscopic pathology of lymph nodes from midstage, simian immunodeficiency virus (SIV)-infected rhesus macaques reveals a highly proliferative pattern consistent with activation of paracortical or germinal center lymphocytes during early and middle stages of SIV infection, which leads to tissue involution during terminal disease (1, 2). *In situ* hybridization studies confirmed the localization of viral RNA in lymph node paracortical lymphocytes, periarteriolar lymphoid sheath cells in the spleen, and the thymic medulla (3). Viral RNA can be detected in lymph nodes even during the acute infection phase within the first few weeks after inoculation (4). Studies in human tissue specimens have identified active and latent human immunodeficiency virus type 1 (HIV-1) infection in lymph nodes (5, 6) and suggested a pattern of progressive changes in lymph node architecture and HIV-1 RNA distribution (6, 7). The terminal phase in HIV-1 disease is characterized by lymph node burnout and general destruction of immune tissues (8); this process reflects the high viral replication rates and extensive destruction of CD4+ lymphocytes (9, 10). Previous studies provided a detailed description of virological and immunological events within individual lymphoid tissues. New techniques are required to study patterns of infection and host response that occur throughout the body.

Noninvasive imaging technologies are used increasingly in clinical medicine. Magnetic resonance imaging and computed tomography are often used for the patient with AIDS to diagnose *Nocardia asteroides* infection (11), brain abnormalities (12, 13), toxoplasmosis (14), and cytomegalovirus infections in the central nervous system (15). Toxoplasmosis, AIDS-associated myocarditis, abnormal bowel activity, and lymphocyte infiltration of salivary glands have been studied using ^{67}Ga-citrate (16–18). We applied the method of positron emission tomography (PET) imaging using 2-^{18}F-2-deoxyglucose (FDG) as the radiotracer to study lymphoid tissue activation during SIV infection in rhesus macaques.

PET imaging is a noninvasive method for evaluating the *in vivo* distribution of a positron-emitting radiotracer. PET-FDG has been used to localize lymphoma within the central nervous system of AIDS patients (19). Based on our previous study of lymphoid tissues in SIV infected rhesus monkeys (1) and unpublished necropsy studies, we concluded that these tissues were highly metabolic and would have elevated FDG uptake similar to solid lymphomas. In this paper, we report the use of PET imaging to visualize the pattern of lymphoid tissue activation in an animal model for AIDS. We are using this technique and comparing the results with data on SIV infection. This preliminary work suggests that this noninvasive whole body metabolic evaluation can be used to monitor the activation of lymphoid tissues that are not readily studied by physical examination, superficial lymph node biopsy, or other imaging modalities.

METHODS

Animals and Virus Inoculation. Animals were selected from the breeding colony of the Wisconsin Regional Primate Research Center (Madison, WI) and screened for retrovirus infections and general health status. Animals were age-matched and included both males and females. Suitable animals were injected intravenously with 10 animal infectious doses (1). Venous blood samples were collected biweekly to monitor infection status and serum antibody to SIV. All infected animals in these studies were seropositive for SIV-specific antibody. Euthanasia was ordered after one animal was moribund for two days and refused food and water, considering that this animal experienced a 34% loss of body weight and had extreme dermatitis. Euthanasia was by sodium pentobarbitol overdose. No animals in this study had diarrhea during the course of infection.

Abbreviations: SIV, simian immunodeficiency virus; PET, positron emission tomography; FDG, 2-^{18}F-2-deoxyglucose.

§To whom reprint requests should be addressed at: University of Wisconsin, Department of Pathology and Laboratory Medicine, 1300 University Avenue, Madison, WI 53706

PET Imaging. Each animal was fasted for a minimum of 6 hr before injection of the radiotracer. A restraint dose of ketamine-HCl was followed by ketamine-xyline and atropine for maximum anesthesia. Approximately 5 mCi of FDG were injected into each 4-kg animal via the saphenous vein. FDG was allowed to distribute for 45–60 min before scanning. The animal was restrained on a Plexiglas board and placed supine in the GE Advance PET scanner (General Electric Medical Systems) with an in-plane resolution of ≈4 mm. Emission data were acquired at four bed positions for 15 min each. Thirty-five transaxial images were obtained at each bed position (a 15-cm axial field of view) for a total coverage of 60-cm body length. Data were reconstructed, reformatted, and viewed in the transaxial, cranial, and sagittal planes.

Biopsy and *in Situ* Hybridization. Tissues were removed after ketamine anesthesia. Lymph node specimens were placed in freshly prepared, buffered formalin for 5 hr and then embedded in paraffin at 60°C. *In situ* hybridization studies were performed by Molecular Histology (Gaithersburg, MD).

Purification of Lymphocyte Subsets from Tissue Specimens. Individual lymphocyte subsets were purified by positive selection using magnetic bead affinity chromatography. Biotinylated, subset specific antibodies included mouse anti-human CD2 (PharMingen) and mouse anti-human CD4, CD8, and CD20 (Becton Dickinson). We confirmed previously that these antibodies crossreact with homologous rhesus cell surface markers. A second layer of biotinylated goat anti-mouse antibody (Olympus, New Hyde Park, NY) was required to increase the efficiency of CD20+ cell purification. Labeled cells were incubated with iron-conjugated streptavidin beads (Miltenyi Biotec, Sunnyvale, CA) and run over a magnetic separation column. Unbound cells were removed by three

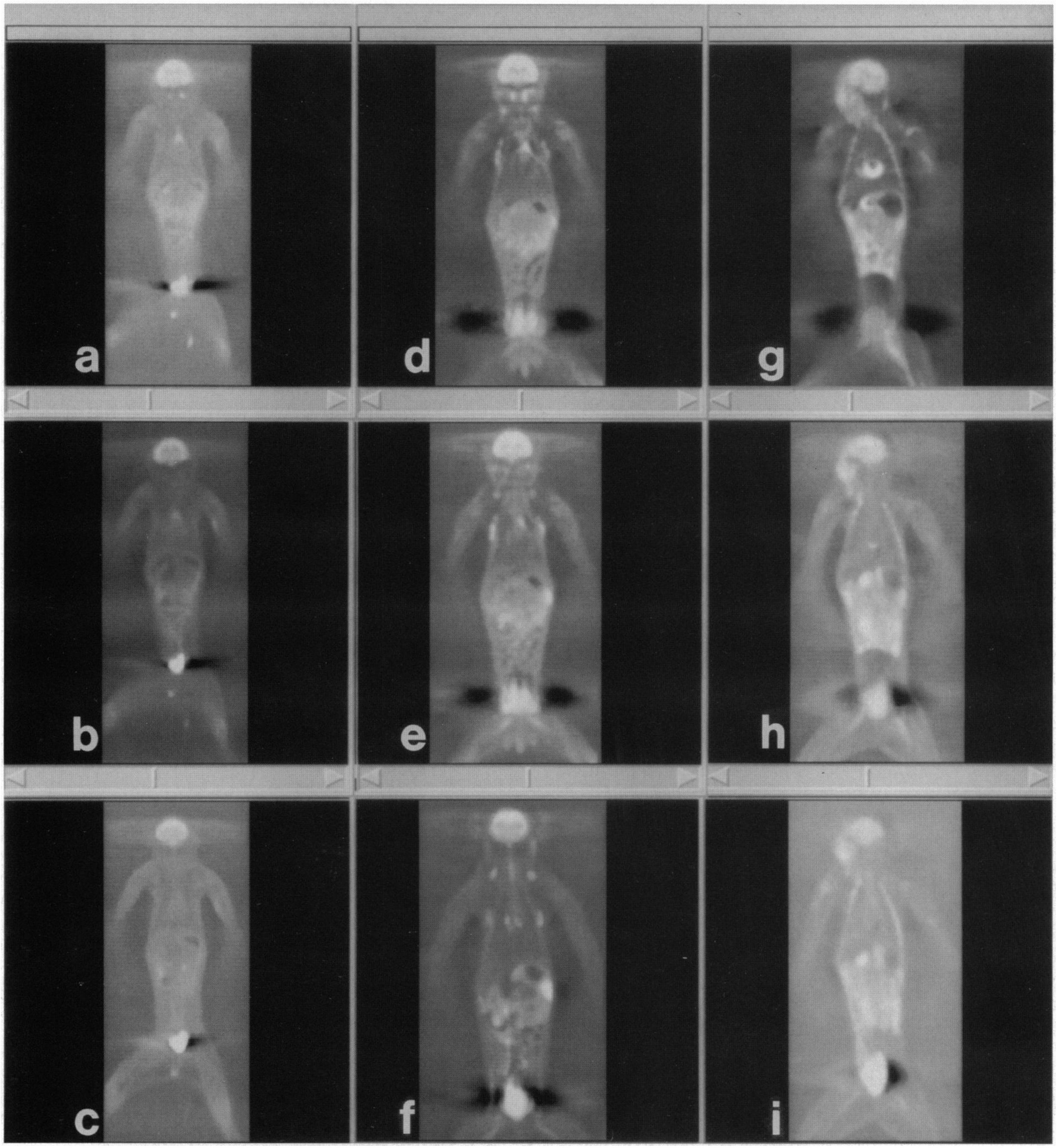

FIG. 1. Three selected coronal planes of PET-FDG images, anterior to posterior, of an uninfected control rhesus macaque monkey (*a*, *b*, and *c*), an SIV-infected monkey in midstage disease (*d*, *e*, and *f*), and an animal with terminal SIV disease (*g*, *h*, and *i*).

washes, and the bound cells were eluted after the magnet was removed.

RESULTS

Rhesus macaques were intravenously infected with SIVmac (251 biological isolate; ref. 20). We compared the whole body PET scans for one uninfected macaque, three infected animals with midstage disease (seropositive for SIV; CD4 cells, <200 cells/μl; intermittent skin rash; no significant weight loss; and mean virus burden, 2.3×10^6 viral RNA copies per ml of plasma), and one animal with terminal disease (extensive psoriatic rash; $>35\%$ decrease in body weight; CD4 cells, <5cells/μl; and virus burden, 9.9×10^7 copies of viral RNA per ml of plasma). A total of seven imaging experiments were performed during this initial study.

Representative PET images are shown in Fig. 1. Each panel in Fig. 1 displays emission data reformatted in the coronal plane (coronal plane thickness of 4 mm). Three representative coronal planes are displayed for one uninfected macaque (*a–c*), one animal with midstage disease (*d–f*), and one animal with terminal disease (*g–h*). In the uninfected animal, two bright spots present just below the brain (*a*) appear to be lymphoid tissues. FDG uptake was noted in the thymus (Fig. 1*a*, delta-shaped structure near the midline in the upper chest). The widest part of the torso contains a dark ellipse in the animal's left upper quadrant representing the gastric bubble. FDG present in the renal calyces was due to urinary excretion of the radiotracer. The bladder frequently showed high radiotracer content in all of our scans despite attempts to drain the urine with an indwelling catheter. Further, we were able to identify FDG uptake in bone marrow, especially the lumbar spine (data not shown). Other lymphoid organs or tissue sites in the uninfected animal demonstrated relatively low amounts of FDG uptake.

A very different pattern of FDG uptake was observed in the animal with midstage SIV disease (*d–f*) 2 months after intravenous inoculation with SIVmac. This monkey had 191 CD4+ T cells/μl of blood and was strongly positive for virus, as judged by infectious cell assay (10^3 infectious cells in 10^6 peripheral blood mononuclear cells) and plasma viremia ($>10^3$ tissue culture infectious doses per ml of plasma). High FDG uptake was observed in the areas of cervical and axillary lymph nodes (*d* and *e*). The axillary lymph nodes appeared as discrete chains that were palpable upon physical examination. A bright signal was observed for the thymus in this 3-year-old, juvenile rhesus macaque (*d*). The mediastinal lymph node cluster was clearly visualized in a position posterior to the thymus (*f*). High FDG uptake was observed in the spleen (just below the gastric bubble in Fig. 1*f*). Other regions of FDG uptake including mesenteric and ileocaecal lymph nodes, are best shown in Fig. 1*f*; the ileocaecal lymph nodes appear near the conjunction of ileum and caecum. The structure we term ileocaecal lymph node, based on anatomic localization, refers to the superior and inferior ileocolic lymph nodes with additional lymphoid tissue attached to the bowel at the ileocaecal junction. FDG uptake was also clearly visualized in the small intestine, and a bright signal was obtained from the popliteal lymph nodes (not displayed in these projections).

Table 1. Distribution of FDG in lymphocyte subsets purified from a single lymph node biopsy.

Cell marker	Cell type	No. of cells recovered	cpm per 10^7 cells
CD2	T cell	1.9×10^7	326
CD4	Helper T cell	0.6×10^7	513
CD8	Cytotoxic T cell	0.5×10^7	808
CD20	B cell	0.45×10^7	3651

The animal was previously injected intravenously with FDG and subjected to PET scanning.

PET images for animals with midstage disease were generally similar to the example presented here. Axillary and inguinal lymph nodes appeared bright in the PET-FDG image and were palpable at the same time. Superficial lymph nodes that were previously recorded by physical examination as palpable and were described as diminished or "burned out" at the time of imaging were not observed by PET-FDG. Differ-

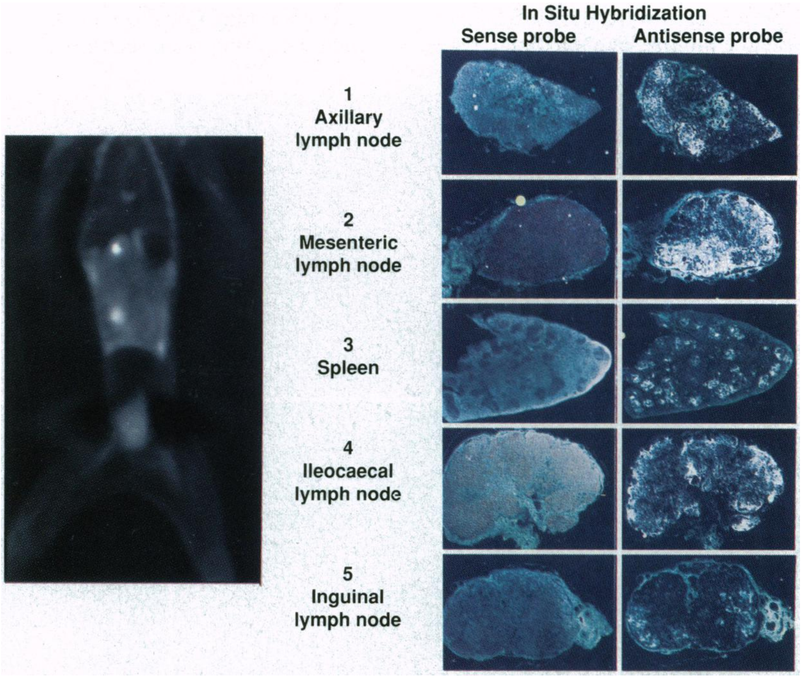

FIG. 2. Combined autopsy and *in situ* hybridization study of rhesus macaque with terminal SIV disease. Sampling sites are described in the text and are identified here by name. The control (sense orientation probe) and antisense hybridization specimens were photographed with epifluorescent light at ×25 magnification. Positive hybridization to SIV RNA is revealed as white dots on the dark background in these photomicrographs under epifluorescent light.

ences among midstage infected animals were most notable in the number and signal intensity for mesenteric lymph nodes, signal intensity for spleen, and size and intensity of images in the ileocaecal region. Some differences were observed for PET-FDG signal intensity in the transverse colon though this was not related to any known enteropathy or active opportunistic infection. Overall, midstage infected animals were characterized by simultaneous presence of PET-FDG signals in superficial and deep lymphoid tissues, whereas late stage animals had few or no visible signals for superficial lymphoid tissues. Repeated PET scans of macaques with midstage disease done up to 7 weeks apart yielded nearly identical results (data not shown), indicating that these findings were reproducible.

An animal with terminal SIV disease was examined by PET scanning on the day before euthanasia. The animal had no CD4+ cells per μl of blood and high plasma virus titers (9.9×10^7 viral RNA copies per ml of plasma). The animal was leukopenic, and had severe wasting, with 34% loss of body weight in the 45 days preceding this experiment. Peripheral lymph nodes were not palpable during physical examination. Images of the head (Fig. 1 *g–i*) are blurred because head movement occurred when brain images were being collected. We did not observe cervical or axillary lymph nodes even when additional images were collected after readministering the anesthetic. Signals are present bilaterally in the upper chest, likely representing bone marrow activity in the ribs. Very high uptake of FDG was present in the myocardium (Fig. 1*g*), which was present to a significantly lower degree in the fasting animals with less advanced disease. At autopsy the heart of the animal appeared ischemic. The spleen was not visualized even though this tissue was normal in size. Two sites of high FDG uptake were noted in the abdomen (Fig. 1*h*) and were identified as mesenteric (upper) and ileocaecal (lower) lymph nodes.

A few hours after scanning one animal with midstage disease, a biopsy was performed to remove the PET-positive, axillary lymph node. The node tissue was disrupted mechanically and mononuclear cells were purified. Individual lymphocyte subsets were labeled with ferritin-conjugated subset-specific antibodies and the populations were purified by positive selection on magnetic bead columns. The purified CD4+ T cells, CD8+ T cells, and the CD20+ B cells were placed in a scintillation counter and the counts per minute per cell were determined (Table 1). In this example, the highest FDG labeling was in B cells. The CD4+ and CD8+ T-cell subpopulations both were radioactively labeled but to only 20% specific activity of the B cells.

The relationship between FDG uptake and virus infection was investigated further in the animal with terminal SIV disease (shown in Fig. 1 and expanded in Fig. 2). At autopsy, individual lymphoid tissues were removed from areas of high and low FDG uptake. The tissues were fixed in formalin and paraffin-embedded for microscopic pathology and *in situ* hybridization. The tissues for *in situ* hybridization were protease pretreated to digest the viral coat and expose viral genomic RNA in addition to viral mRNA that would be expected for active SIV replication. As seen in Fig. 2, tissues that were not visible on the PET-FDG image included axillary lymph nodes, inguinal lymph nodes, and spleen. These PET-FDG-negative tissues showed diffuse follicular and paracortical lymphocyte depletion with mild histiocyte proliferation. Photomicrographs from *in situ* hybridization experiments with spleen, right axillary node, and right inguinal node showed a low level of SIV RNA. Some SIV RNA was present in germinal centers of the spleen and could be due to virus particles trapped there. Viral RNA in the axillary lymph node was present in a small portion of the tissue, and the pattern was consistent with what would be expected for a partially involuted tissue. The ileocaecal node and one mesenteric node showed high FDG uptake. Histopathology revealed intact lymph node architecture with high cellularity and highly proliferative B-cell zones. Photomicrographs showed widely distributed SIV RNA in the ileocaecal and mesenteric lymph nodes. In this terminal animal, virus was readily isolated from purified mononuclear cells in the ileocaecal node despite a peripheral blood CD4 count of 0 CD4+ cells/μl; virus was readily isolated from plasma. The thymus was not visualized on PET imaging. Histopathology and *in situ* hybridization studies of the thymus revealed mostly connective tissue with little thymic cortex or medulla and no evidence for active SIV replication (data not shown).

Higher magnification images of the spleen, axillary, and inguinal lymph node sections from *in situ* hybridization studies

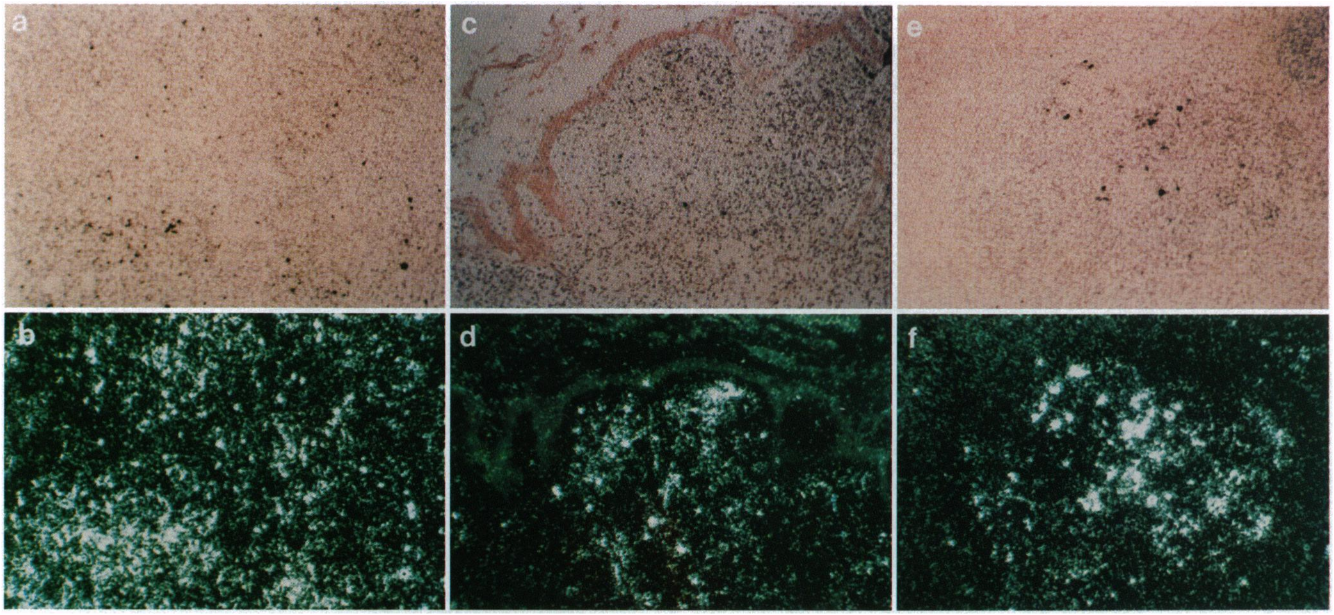

FIG. 3. Higher-power (×100 magnification of the specimen) photomicrographs of *in situ* hybridization patterns for SIV antisense probe in ileocaecal lymph node (*a* and *b*), inguinal lymph node (*c* and *d*), and spleen (*e* and *f*). (*a*, *c*, and *e*) Photographs with bright field illumination where autoradiography grains appear dark. (*b*, *d*, and *f*) Photographs with epifluorescent light where grains appear as white dots on a dark background.

confirmed the differences in viral RNA distribution (Fig. 3). The SIV RNA is identified by black grains in the bright field photomicrographs (Fig. 3 *a*, *c*, and *e*) that were enhanced under epifluorescent light (*b*, *d*, and *f*). When compared with the inguinal node and spleen, the ileocaecal node (*a* and *b*) possessed multiple centers of heavy black grains with a diffuse distribution of light granularity throughout the tissue.

DISCUSSION

Our knowledge of viral pathogenesis in AIDS is based primarily on natural history studies of HIV infection in man, *in vitro* models for virus replication and cell killing, and evaluation of virus replication *in vivo* using blood samples and lymph node biopsy specimens. A picture emerges of an aggressive pathogen that mounts a broad attack on lymphoid tissues, resulting initially in a peripheral generalized lymphadenopathy (21, 22) that eventually leads to destruction of lymphoid tissues (6, 7, 23) and immune dysfunction. We used positron emission tomography imaging with FDG in a living animal after SIV infection. PET imaging with FDG provided a new view of lymphoid tissue activation and showed the extent of immune response to virus reflecting the widely distributed sites of virus replication. In the case of a terminal animal with wasting and peripheral lymph node burnout, significant metabolic activity was detected in midgut lymphoid tissues, particularly the mesenteric and ileocaecal lymph nodes. Microscopic pathology of these tissues showed the typical diffuse paracortical and germinal center lymphocyte proliferation that we expect for activated lymph nodes in SIV infection.

The ileocaecal lymph node is not remarkable in uninfected animals but is a prominent feature in SIV infection. Review of 12 necropsies for SIV-infected rhesus at the Wisconsin Regional Primate Research Center showed highly activated ileocaecal lymph nodes in each case (unpublished observations). This is especially significant inasmuch as 10 of these animals had superficial lymph node involution with acute wasting and six of the animals were confirmed by flow cytometry as having 0 CD4+ T cells/μl in peripheral blood. The combined PET imaging and autopsy study presented here showed high-level virus replication as judged by *in situ* hybridization. Further, we easily isolated SIV from mononuclear cells in the lymph node that were most likely CD4+ T cells. The PET-FDG study of one animal with terminal disease showed an interesting correlation between lymphoid tissue destruction and increasing levels of plasma viremia. In other autopsy cases that appeared similar to the terminal animal studied here (data not shown), we noted elevated plasma viremia ($>10^7$ viral RNA copies/ml of plasma) in the context of extensive lymphoid tissue depletion with the important caveat that highly activated ileocaecal lymph nodes were present in each case. It appears that virus levels in plasma is controlled effectively when a intact reticuloendothelial system is present, even though the absolute capacity to replicate virus should be higher when a greater amount of lymphoid tissue is present. These data suggest that virus burden in blood may reflect the combined rates of virus replication and virus clearance by lymphoid tissues, and further studies are required to understand correlations between plasma viral RNA and virus dynamics.

Disease progression has been linked previously to decreases in peripheral blood CD4+ T cells and to increased numbers of infected cells or cell-free virus particles in peripheral blood (24–28). Biopsy specimens have shown the relationship between progressive lymph node involution and disease progression (7, 23). This preliminary work suggested that application of a noninvasive method for whole body imaging elucidated a metabolic profile reflecting virus infection, dissemination, and lymphoid tissue activation. Our studies show that widespread lymphoid tissue activation with significant involvement of the spleen is a feature of midstage disease. Terminal disease is characterized by a loss of activity in spleen and superficial lymph nodes, even though deep lymphoid tissues, most notably the ileocaecal lymph node and mesenteric lymph nodes, remain active. It was surprising to find that a substantial amount of lymphoid tissue remained highly active in animals with no evidence of peripheral blood CD4+ T cells. The ileocaecal lymph node is highly infected in late stage disease and, considering its anatomic location, could play a important role in terminal disease progression with a significant effect on wasting disease. Preliminary studies of seven HIV-positive patients with low CD4+ T cells in blood also showed activated tissues in the ileocaecal region and patterns of signal intensity similar to those observed here for SIV-infected rhesus macaques. These findings provide hope that even late stage patients retain some components of active lymphoid tissue and could benefit from therapies designed to reconstitute immunity.

This study represents manuscript number 36-008 from the Wisconsin Regional Primate Research Center. This study was supported by grants from the National Council for Research Resources (Grant RR00167, Primate Center Supplemental Funds for AIDS Research) and the National Institute for Allergy and Infectious Diseases (Grants AI24591 and AI36643, to C.D.P.).

1. Pauza, C. D., Emau, P., Salvato, M. S., Trivedi, P., MacKenzie, D., Malkovsky, M., Uno, H. & Schultz, K. T. (1993) *J. Med. Primatol.* **22,** 154–161.
2. Letvin, N. L. & King, N. W. (1990) *J. Acquired Immune Defic. Syndr.* **3,** 1023–1040.
3. Lackner, A. L., Vogel, P., Ramos, R. A., Kluge, J. D. & Marthas, M. (1994) *Am. J. Pathol.* **145,** 428–439.
4. Reimann, K. A., Tenner-Racz, K., Racz, P., Montefiori, D. C., Yasutomi, Y., Lin, W., Ransil, B. J. & Letvin, N. L. (1994) *J. Virol.* **68,** 2362–2370.
5. Embretson, J., Zupancic, M., Ribas, J. L., Burke, A., Racz, P., Tenner-Racz, K. & Haase, A. T. (1993) *Nature (London)* **362,** 359–362.
6. Pantaleo, G., Graziosi, C., Butini, L., Pizzo, P. A., Schnittman, S., Kotler, D. P. & Fauci, A. S. (1991) *Proc. Natl. Acad. Sci. USA* **88,** 9838–9843.
7. Racz, P., Tenner-Racz, K., Kahl, C., Feller, A., Kern, P. & Dietrich, M. (1986) *Prog. Allergy* **37,** 81–181.
8. Pantaleo, G., Graziosi, C., Demarest, J. F., Cohen, O. J., Vaccarezza, M., Gantt, K., Muro-Cacho, C. & Fauci, A. S. (1994) *Immunol. Rev.* **140,** 105–130.
9. Ho, D. D., Neumann, A. U., Perelson, A. S., Chen, W., Leonard, J. M. & Markowitz, M. (1995) *Nature (London)* **373,** 123–126.
10. Wei, X., Ghosh, S. K., Taylor, M. E., Johnson, V. A., Emini, E. A., Deutsch, P., Lifson, J. D., Bonhoeffer, S., Nowak, M. A., Hahn, B. H., Saag, M. S. & Shaw, G. M. (1995) *Nature (London)* **373,** 117–122.
11. LeBlang, S. D., Whiteman, M. L., Post, M. J., Uttamchandani, R. B., Bell, M. D. & Smirniotopolous, J. G. (1995) *J. Comput. Assist. Tomogr.* **19,** 15–22.
12. Mechtler, L. L. & Kinkel, P. R. (1993) *Curr. Opin. Neurol.* **6,** 912–918.
13. McConnell, J. R., Swindells, S., Ong, C. S., Gmeiner, W. H., Chu, W. K., Brown, D. K. & Gendelman, H. E. (1994) *AIDS Res. Hum. Retroviruses* **10,** 977–982.
14. Castillo, M. (1994) *Top. Magn. Reson. Imaging* **6,** 3–10.
15. Nagamitsu, S., Okabayashi, S., Dai, S., Morimitsu, Y., Murakami, T., Matsuishi, T., Motizuki, M. & Kato, H. (1994) *Intern. Med.* **33,** 158–162.
16. Memel, D. S., DeRogatis, A. J. & William, D. C. (1991) *Clin. Nucl. Med.* **16,** 315–317.
17. Slizofski, W. J., Brown, S. J., Dadparvar, S. & Glab, L. B. (1991) *Clin. Nucl. Med.* **16,** 473–477.
18. Rosenberg, Z. S., Joffe, S. A. & Itescu, S. (1992) *Radiology* **184,** 761–764.
19. Hoffman, J. M., Waskin, H. A., Schifter, T., Hanson, M. W., Gray, L., Rosenfeld, S. & Coleman, R. E. (1993) *J. Nucl. Med.* **34,** 567–575.
20. Daniel, M. D., Letvin, N. L., King, N. W., Kannagi, M., Sehgal, P. K., Hunt, R. D., Kanki, P. J., Essex, M. & Desrosiers, R. C. (1985) *Science* **228,** 1201–1204.

21. Kaplan, J., Spira, T., Fishbein, D., Pinsky, P. & Schonberg, L. (1987) *J. Am. Med. Assoc.* **257,** 335–337.
22. Ioachim, H., Lerner, C. & Tapper, M. (1983) *J. Am. Med. Assoc.* **250,** 1306–1309.
23. Garcia, C. F., Lifson, J. D., Engleman, E. G., Schmidt, D. M., Warnke, R. A. & Wood, G. S. (1986) *Am. J. Clin. Pathol.* **86,** 706–715.
24. Saag, M. S., Crain, M. J., Decker, W. D., Campbell-Hill, S., Robinson, S., Brown, W. E., Leuther, M., Whitely, R. J., Hahn, B. H. & Shaw, G. M. (1991) *J. Infect. Dis.* **164,** 72–80.
25. Lee, T. H., Sheppard, H. W., Reis, M., Dondero, D., Osmond, D. & Busch, M. P. (1994) *J. Acquired Immune Defic. Syndr.* **7,** 381–388.
26. Katzenstein, D. A., Holodniy, M., Israelski, D. M., Sengupta, S., Mole, L. A., Bubp, J. L. & Merigan, T. C. (1992) *J. Acquired Immune Defic. Syndr.* **5,** 107–112.
27. Daar, E. S., Moudgil, T., Meyer, R. D. & Ho, D. D. (1991) *New Engl. J. Med.* **324,** 961–964.
28. Coombs, R., Collier, A., Allain, J.-P., Nikora, B., Leuther, M., Gjerset, G. & Corey, L. (1989) *New Engl. J. Med.* **321,** 1626–1631.